Effects of calreticulin deficiency and myeloproliferative neoplasm (MPN)-linked mutation on cellular calcium signaling

Ishmael Nii Ayibontey Tagoe[1, 2], **Amanpreet Kaur** [1], **Osbourne Quaye**[2], **Emmanuel Ayitey Tagoe**[4], **Nicole Koropatkin**[1], **Leslie S. Satin**[3], **and Malini Raghavan**[1]*

[1]Departments of Microbiology and Immunology and [3]Pharmacology,

University of Michigan Medical School, Ann Arbor, MI

[2]West African Centre for Cell Biology of Infectious Pathogens,

Departments of Biochemistry, Cell and Molecular Biology, and

[4]Medical Laboratory Sciences, University of Ghana

*Correspondence to Malini Raghavan, PhD: malinir@umich.edu

ABSTRACT

Calreticulin (CRT) is an endoplasmic reticulum (ER) chaperone containing multiple low affinity calcium-binding sites in its acidic C-terminal domain. Somatic mutations of the CRT gene (*CALR*) that are drivers of a subset of myeloproliferative neoplasms (MPN) alter the C-terminal domain. Perturbations in ER calcium storage and signaling are reported for an MPN type I mutant, CRT_{Del52}, and have been linked to disease pathogenesis. The effects of the mutations on calcium binding are, however, yet to be quantified. Using recombinant purified proteins, we found that residues 340-349 in the CRT C-terminal domain, conserved in both the wild-type CRT and CRT_{Del52}, are major contributors to low affinity calcium binding measured using isothermal titration calorimetry (ITC). Quantitative measurements in various engineered cell lines also indicate overall similarities in ER and cytosolic calcium levels and signals in CRT knockout (CRT-KO) cells reconstituted with wild-type CRT or CRT_{Del52}. Notably, the CRT-KO induces transcriptional changes to various genes in the cellular calcium signaling pathways. Thus, CRT_{Del52} retains at least some low affinity calcium binding sites, and any measured effects of ER and cytosolic calcium signal changes in cells with CRT perturbations may not be solely determined by its calcium binding functions.

Introduction

Calreticulin (CRT) is an endoplasmic reticulum (ER) luminal protein that has been found to play key roles in the assembly and folding of N-linked glycoproteins. CRT has an N-terminal globular domain that contains a glycan binding site and a single high affinity calcium binding site, an extended P domain that is involved in co-chaperone binding, and a highly acidic C-terminal domain that contains multiple low affinity calcium binding sites (1-4). As an ER chaperone, CRT is thought to play a critical role in maintaining cellular calcium homeostasis (5). The ER has a relatively high free calcium concentration of 0.5-1 μM through the presence of various low affinity calcium-binding proteins that buffer calcium, whereas cytosolic calcium levels are maintained within a narrow range of around 100 nM (5). The maintenance of calcium homeostasis within cellular compartments is essential for cell function and survival (6). Early studies have shown that the C-domain of CRT contributes to ER calcium storage, and ER calcium levels are reduced in cells lacking CRT (3).

Somatic mutations of exon 9 of the *CALR* gene including a 52-base pair deletion (Del52; type 1 mutation) and a 5-base pair insertion (Ins5; type 2 mutation), are driver mutations in some myeloproliferative neoplasms (MPN), specifically in essential thrombocythemia (ET) and primary and secondary myelofibrosis (PMF) (7, 8). The MPN mutations change the CRT C-domain residues from being predominantly acidic to a high prevalence of basic amino acids and result in a loss of the ER-retention KDEL sequence (7, 8). Although all MPN CRT mutants change the sequence and charge of the C-domain, a greater number of acidic residues are retained in MPN type 2 mutant (CRT_{Ins5}), compared to the type I mutant (CRT_{Del52}). The loss of more acidic residues from the C-terminal domain of CRT_{Del52} has been reported to impair its calcium binding and reduce ER calcium levels (9). Store-operated calcium entry (SOCE) is a physiological process that allows for the entry of extracellular calcium and ER calcium restoration following ER calcium depletion (10, 11). Altered calcium release from the ER and SOCE was reported for MPN type I but not type 2 mutants in cultured megakaryocytes from MPN patients (12). In another study, spontaneous calcium spikes and increased SOCE activation were observed in cultured megakaryocytes from MPN type I and type 2 mutants when compared to healthy donors (13).

Although global calcium binding defects were noted for CRT_{Del52} (9) and altered cellular calcium signaling were also reported (12, 13), it remains unclear whether MPN-linked CRT_{Del52} has any low affinity calcium binding capacity, given that a few conserved acidic residues are retained in its C-domain (Figure 1). In fact, our previous studies showed that a truncated version of murine wild-type CRT (mCRT) containing the non-mutated part of CRT_{Del52} and two additional C-terminal residues ($mCRT_{1-351}$) showed similar low affinity calcium binding characteristics as the wild-type mCRT (14). On the other hand, further truncation of mCRT ($mCRT_{1-339}$) was needed to fully disrupt calcium binding (14, 15). The goal of the current study was to measure low affinity calcium binding by CRT_{Del52} compared with wild-type human CRT. We used isothermal titration calorimetry to quantify calcium binding of recombinant, purified wild-type CRT and its mutants. Additionally, using ratiometric ER and cytosolic calcium probes, and flow cytometry or live cell imaging, calcium levels were measured in CRT-KO cell lines compared to the parental cells, and the CRT-KO cells reconstituted with either wild-type CRT or CRT_{Del52}. Furthermore, sarco(endo)plasmic reticulum (SERCA) inhibitor-induced changes to cytosolic and ER calcium levels and store-operated calcium entry (SOCE) were assessed. Finally, to better understand whether the CRT-KO can affect cellular calcium signaling through mechanisms other than its low affinity calcium binding

functions of CRT, we undertook bulk RNA sequencing of wild-type vs. CRT-KO cell lines. We identified numerous calcium signaling pathway-related transcriptional changes in CRT-deficient cells compared to wild-type cells that could contribute to ER and cytosolic calcium changes in CRT-KO cells.

Material and Methods

DNA constructs

Wild type human CRT (accession number P27797) was expressed as a fusion protein with the B1 domain of streptococcal protein G (GB1) (16) and hexa-histidine tag using the pGB1 vector via ligation-independent cloning, as described (17). Using the pGB1- h*CALR* plasmid as a template, constructs for expressing his-tagged CRT $_{(1\text{-}351)}$ and CRT $_{(1\text{-}339)}$ truncation mutants were generated using QuickChange Site-Directed Mutagenesis Kit (Agilent Technologies) following the manufacturer's protocol and using primers indicated in the Supplemental Table 1**.** The sgRNA for CRT knockdown was designed to target the GGCCACAGATGTCGGGACCT sequence found at the boundary of intron 3 and exon 4 of the *CALR* gene (18). The primers for cloning of sgRNA into pLentiCRISPRv2-BLAST (pLB) vector are given in the supplemental Table 1. The pMSCV constructs used for mammalian expression of wild type CRT and the CRT_{Del52} described earlier (19) were used as templates to subclone wild type *CALR* and $CALR_{Del52}$ into pSIP-*ZsGreen* (pLVX-SFFV-IRES-Puro) vector (20) at the EcoRI and NotI sites using primers given in the supplemental table1. The pSIP-$CALR_{Del52\text{-}KDEL}$construct containing a C-terminal KDEL motif was generated using pSIP-$CALR_{Del52}$ as a template and primers given in Supplemental Table 1. The amplicons were cloned at the EcoRI and NotI sites in the pSIP vector. The cloning of *CALR* genes at the EcoRI and NotI sites within the pSIP-*ZsGreen* vector resulted in the removal of a fragment carrying *ZsGreen* so that the transduced cells did not express ZsGreen.

Protein expression and purification

Wild-type CRT, CRT_{Del52} and the truncated mutants were purified on nickel resin as described previously (14). Chemically-competent Origami B(DE3) *E. coli* cells were transformed with the pGB1 constructs of wild type CRT, $CRT_{(1\text{-}351)}$, $CRT_{(1\text{-}339)}$ and $CRT_{Del52,}$ and grown for 16 hours overnight at 37°C. The overnight primary cultures were inoculated into larger volumes of LB media and grown in a shaking incubator at 220 rpm and 37°C until the OD_{600} of 0.8. Protein expression was then induced with 200 µM IPTG, and the cultures were further incubated at 16°C overnight on shaking. The bacterial cells were harvested, pelleted, and lysed in 50 mL of HEPES buffer containing (20 mM HEPES pH 7.5, 140 mM NaCl, 1 mM $CaCl_2$) by sonication. The lysates were clarified by centrifugation at 10,000 rpm, 4°C for 30 minutes. The supernatant was incubated with nickel-NTA resin (Qiagen, 1018244) for 3 hours at 4°C and purified through a gravity-flow column. The unbound proteins and contaminants were removed by washing with a wash buffer containing 20 mM HEPES pH 7.5, 140 mM NaCl, 1 mM $CaCl_2$, 10 mM imidazole and the his-tagged CRT proteins were eluted with elution buffer containing 20 mM HEPES pH 7.5, 140 mM NaCl, 1 mM $CaCl_2$, 350 mM imidazole. The eluted proteins were concentrated and subjected to fast protein liquid chromatography (AKTA-go) on a Superdex 200 increase 10/300 GL column at 4°C to obtain the corresponding monomer fractions. The monomer fractions were then pooled and concentrated to 4 mg/mL using Amicon ultra concentrators with a molecular weight cut-off of 30,000 Dalton (Millipore). This fraction was used for isothermal titration calorimetry (ITC) measurement.

Isothermal titration calorimetry

Isothermal titration calorimetry (ITC) measurements were done using the Nano-ITC SV (TA Instruments). As described previously (14), purified monomers of wild-type CRT and mutants at 100 μM were initially pre-incubated with 50 μM $CaCl_2$ in 20 mM HEPES, 10 mM NaCl for 30 minutes to block the high affinity calcium binding sites. This was followed by titrating 10 mM $CaCl_2$ in 20 mM HEPES, 10 mM NaCl into 100 μM solution of proteins at 37°C. The heat change measured for each of the 25 sequential injections was curve-fitted to calculate the enthalpy, moles per binding site, and the dissociation constant using NanoAnalyze software.

Cell culture, viral transduction and reconstitution of the expression of CRT mutants

Megakaryoblastic leukemia cell line (MEG-01) from ATCC and Human embryonic kidney (HEK) 293T cell lines were cultured and maintained in RPMI 1640 and DMEM media, respectively, supplemented with 10% heat inactivated fetal bovine serum (FBS, Gibco), antibiotic/antimycotic solution containing penicillin, streptomycin and amphotericin (15240062) respectively at 37°C, 5% CO_2 and 95% humidity. Wild type CRT was knocked out in MEG-01 cells and HEK293T cells (CRT-KO) using Cas9 and single guide RNA (sgRNA) targeting GGCCACAGATGTCGGGACCT sequence within the *CALR* gene. For CRISPR/Cas9 mediated CRT knockdown, the HEK293T cells were first transfected with the lentiviral construct containing CRT-targeting sgRNA (pLB-*CRT* sgRNA) or the empty pLB vector along with the psPAX2 and MD2.G vectors using Lipfectamine™ LTX with PLUS™ reagent (Invitrogen) to make lentivirus. The lentivirus-containing media were harvested, filtered with 0.45 μm syringe filters and added onto the target cells (MEG-01 or HEK293T cells) for infection. The MEG-01 cells were infected by spinoculation at 2500 rpm for 2 hours at room temperature in the presence of polybrene (8 μg/mL), followed by replacement of 80% of virus-containing media with fresh complete media. For HEK293T cells, the harvested viral supernatant was added to HEK 293T cells and incubated for 2 hours at 37°C, after which 80% of the viral suspension was replaced with complete growth media. Virus-containing media was completely replaced with fresh growth media 24 hours after infection, and the drug selection started with 2.5 μg/mL blasticidin 48 hours post-infection. Following drug selection, the CRT-KO cells were plated at a dilution of one cell per well in a 96-well plate to isolate single-cell clones. The selected single-cell clones of CRT-KO MEG-01 and HEK293T cells were subsequently reconstituted with wild-type human CRT, CRT_{Del52}, or CRT_{Del52} with a C-terminal KDEL sequence using the respective pSIP constructs and the same method of transduction explained above. The cells transduced with the empty pSIP vector without *ZsGreen* (Supplemental Table 1) were also generated to serve as control cells. Cells expressing CRT proteins or those containing empty pSIP vector were selected with 2 μg/mL puromycin. Selected cells were expanded and used for ER calcium measurements.

Immunoblotting

The HEK293T and MEG-01 cells were harvested and lysed in lysis buffer (50 mM Tris pH 7.5, 150 mM NaCl, 1% Triton X-100, 5 mM $CaCl_2$) for 30 minutes at 4°C. The lysates were clarified by centrifugation, and the total amount of protein in the lysates was determined using the BCA reagent kit (Thermoscientific). The volume of lysate containing 20-40 μg of protein was denatured by boiling in 1X SDS loading dye for 5 minutes and subjected to SDS-PAGE. Following electrophoresis, the proteins were transferred onto a PVDF membrane. The membranes were blocked in 5% non-fat dry milk solution in TBST (Tris-buffered saline with Tween-20), followed by immunoblotting and detection for protein expression using primary anti-CRT(N) antibody (Cell

Signaling Technology (CST) 12238, 1:10,000 dilution) for detection of CRT_{WT} and anti-CRT(C-mut) antibody for detection of CRT mutants (19). Anti-GAPDH (CST 2118, 1:20,000 dilution) was used to probe for GAPDH as a loading control. Blots were incubated with horseradish peroxidase-conjugated secondary antibodies (Jackson ImmunoResearch) and developed by chemiluminescence (Pierce™ ECL western blotting substrate, 32106). Immunoblot images were captured using the Azure 300 chemi imager (Azure Biosystems).

Cytosolic calcium measurement and store-operated calcium entry (SOCE) induction

MEG-01 cells were plated on glass coverslips pretreated with 0.01% poly-L-lysine to facilitate cell attachment. Cells were loaded with 2.5 μM Fura-2/AM dye (Ion Biosciences) supplemented with 0.1% pluronic acid in a physiological salt solution (PSS) containing 140 mM NaCl, 2 mM $CaCl_2$, 5 mM KCl, 2 mM $MgCl_2$, 10 mM HEPES and 11 mM glucose, and incubated for 60 minutes at 37°C. Live single-cell imaging was done at 20X magnification using Olympus IX71 inverted microscope equipped with a TILL Polychrome V monochromator light source, a Dual-View emission beam splitter, and a cooled Photometrics Quant-EM camera. Cells were transferred to a perfusion chamber that was mounted on the microscope stage, and PSS with or without 2 mM $CaCl_2$ was flowed over cells using a gravity-fed perifusion system. Cytosolic calcium measurements were performed by perifusing Fura-2 loaded cells in the chamber with 2 mM Ca^{2+}, followed by the addition of 25 μM cyclopiazonic acid (CPA) (Cayman) into the imaging buffer. To determine cytosolic calcium levels after activating SOCE, cells were initially perfused with Ca^{2+}-free PSS containing 0.1 mM EGTA, followed by the addition of 25 μM CPA in Ca^{2+}-free PSS and subsequent addition of 2 mM Ca^{2+} in PSS without EGTA to reestablish calcium influx. Fura-2/AM was excited at 340 and 380 nm, and emission was recorded at 510 nm at 5-second intervals. The emission signals corresponding to the 340 and 380 nm excitation were recorded, and the signals resulting from 340/380 nm excitation were calculated using the Meta Fluor software. The basal cytosolic calcium was defined as the ratio of 340/380 nm signals before CPA treatment. The fractional increase in cytosolic calcium levels after ER Ca^{2+} depletion with CPA was calculated as the difference between maximal and baseline ratios. The fractional increase in cytosolic calcium observed after inducing SOCE and re-adding 2 mM extracellular Ca^{2+} was calculated as the difference between the peak ratio of Ca^{2+} after calcium re-addition and the minimum ratio following ER calcium depletion. Total calcium release after ER Ca^{2+} depletion was reported as the total area under the curve (AUC).

ER calcium measurements in HEK293T cells

Cells were transiently transfected with pCIS-GEM-CEPIA1er ((21); Addgene plasmid # 58217) using Fugene HD reagent (Promega). The transfected cells were harvested after 72 hours. Cells were washed twice with FACS buffer (PBS + 2% FBS) supplemented with 2 mM Ca^{2+} and resuspended in the same FACS buffer. The live-dead stain 7-AAD (BD) was added at 1:200 dilution and the cells were analyzed by flow cytometry using the BD LSRFortessa cell analyzer. The signal for the Ca^{2+}-bound GEM-CEPIA1er probe was recorded in the Pacific Blue channel (excitation at 405 nm and emission at 452-455 nm) and the signal for the unbound probe was recorded in the AmCyan channel (excitation at 405 and emission at 498 nm). The analysis of flow cytometry data was done in the FlowJo software (v10.10.00). The cells were gated based on the forward (FSC-A) and side scatter (SSC-A), followed by gating on the 7AAD-negative (live) cells,

and subsequent gating on the cells positive for the expression of GEM-CEPIA1er probe measured in the Pacific Blue and AmCyan channels. Basal signals were initially recorded, followed by the addition of 5 μM thapsigargin (Tg) and subsequent recording of signals for the treated and untreated cells at four different time points between 2 – 10 minutes. The ratio of mean fluorescence intensity (MFI) of the bound to the unbound signal was used for calculations.

RNA-sequencing

The parental and CRT-KO MEG-01 cells were grown in complete media for 12-18 hours before harvesting. Total RNA was isolated using the RNeasy Plus Mini Kit (Qiagen). This was followed by poly-A selection and enrichment of mRNA using NEB Next Ultra Express RNA kit and a NEB Poly A kit (New England Biolabs). Sequencing was done on the NovaSeq at PE150, targeting 30-40 million reads/sample after cDNA library preparation. The differentially expressed genes were selected as those with a log2 fold-change of <-0.58 or >0.58 and p values <0.05. The results from RNA sequencing were further analyzed in the iPathwayGuide to identify significantly altered proteins related to calcium signaling. The volcano plot was plotted in GraphPad Prism as Log2 fold-change (x-axis) *vs.* -Log10 adjusted p-value.

Statistical analysis

All data were compiled using Microsoft Excel and analyzed using GraphPad Prism 10.4. A Student's t-test was used to compare mean differences between two groups, while a one-way ANOVA was used to compare mean differences among more than two groups. The threshold for statistical significance was observed at a p-value ≤ 0.05.

Results

MPN-linked CRT_{Del52} retained some low affinity calcium binding

Previous studies (14) have implicated residues 340 to 351 of mCRT, which are identical in wild-type human CRT and fully conserved with the 340 to 349 residues of CRT_{Del52}, to be involved in low affinity calcium binding. Further truncation of the C-domain to the residue 339 ($mCRT_{1-339}$) led to the full loss of calcium binding (14). Figure 1 shows a sequence alignment of murine CRT, human CRT, $CRT_{Ins5,}$ and CRT_{Del52} proteins. and indicates that the residues previously implicated in low affinity calcium binding are also shared between wild-type CRT and $CRT_{Del52.}$ Recombinant his-tagged purified proteins were used to compare calcium binding by human CRT and its variants. Chromatograms for human wild type CRT, CRT_{Del52}, $CRT_{(1-339)}$ and $CRT_{(1-351)}$ are shown in Figure 2A. SDS-PAGE gels corresponding to the purified proteins are shown in Figure 2B. CRT_{Ins5} was not purified in sufficient quantities needed for ITC experiments and was not further investigated in this study.

For the ITC measurements, twenty-five sequential injections of $CaCl_2$ were added to solutions containing human wild-type CRT, CRT_{Del52}, or the indicated truncation mutants of wild-type human CRT. The contributions of the high affinity calcium-binding sites to heat changes were eliminated prior to the calcium titrations by blocking with 50 μM $CaCl_2$. Consistent with previous studies with $mCRT_{(1–339)}$, no calcium binding was observed with the human $CRT_{(1–339)}$. However, similar binding profiles and properties were observed with wild-type CRT, $CRT_{Del52,}$ and the $CRT_{(1-351)}$ mutant. Consistent with the previously reported findings of calcium binding characteristics of $mCRT_{(1-351)}$, similar low affinity binding profiles were observed for human $CRT_{(1-351)}$ and wild-type human CRT (Figures 3A-D and Table 1).

Small non-significant differences observed in ER calcium levels between CRT-KO HEK cells reconstituted with wild-type CRT or CRT_{Del52}

While the CRT_{Del52} mutant retains some ability to bind calcium (Figure 3 and Table 1), the loss of the ER-retention KDEL sequence induced by the frameshift mutation, which results in the secretion of the protein from the ER, (19, 22-27) might be expected to cause ER calcium insufficiency in cells expressing CRT_{Del52} compared to wild-type CRT. We investigated ER calcium signals in CRT knock-out HEK293T cells generated by CRISPR/Cas9 gene editing. A clonal KO line was generated and subsequently reconstituted with constructs encoding wild-type CRT, CRT_{Del52}, or CRT_{Del52} with a KDEL sequence added at the C-terminus ($CRT_{Del52\text{-}KDEL}$). Protein expression was assessed by immunoblotting with anti-CRT(N), which detects an N-domain epitope present in all CRT constructs, and anti-CRT(C-mut), which was specifically raised against the mutant CRT C-terminus (19). While the recognition with anti-CRT (N) was very weak in lysates of cells expressing $CRT_{Del52,}$ which is secreted, $CRT_{Del52\text{-}KDEL}$ is readily detectable with both antibodies. Both wild-type CRT and $CRT_{Del52+KDEL}$ were reconstituted to higher levels than in the parental cells (Figure 4A**,** lanes 1 and 2 compared to 7-8 and 11-12). The KO and reconstituted cells were further transfected with pCIS-GEM-CEPIA1er, genetically encodes a ratiometric ER calcium probe (21). Emission signals for calcium-bound (452-455 nm) and unbound (498 nm) probe were measured using flow cytometry in the Pacific Blue and AmCyan channels, respectively, following excitation with the 405 nm (violet) laser. Flow cytometric analysis was undertaken in buffer containing 2 mM extracellular calcium (Figures 4B and 4C). There was a significant decrease in basal free ER calcium, measured by the bound/unbound ratios in CRT-KO

cells compared to the parental cells (Figure 4D, left panel). ER calcium levels were at least partially restored, although non-significantly, when the CRT-KO cells were reconstituted with wild-type CRT. CRT-KO cells reconstituted with CRT_{Del52} and $CRT_{Del52\text{-}KDEL}$ showed small but non-significant decreases in ER calcium levels compared to those reconstituted with wild-type CRT (Figure 4D, right panel). Changes to ER calcium levels in response to thapsigargin (Tg), a SERCA inhibitor, were similar in the parental *vs.* CRT-KO cells, and in the CRT-KO cells compared with those reconstituted with different CRT proteins (Figure 4E).

Similar cytosolic calcium and SOCE signals in a CRT-KO megakaryocyte cell line reconstituted with wild-type CRT or CRT_{Del52}

The strict maintenance of cytosolic calcium levels needed for various cell signaling pathways is regulated by ER calcium buffering and storage, mediated by the transporters, pumps, voltage-gated ion channels, and calcium binding chaperones (5, 28). MPN CRT mutations cause thrombopoietin-independent differentiation of megakaryocytes to platelets via the thrombopoietin receptor (MPL) (22, 24, 25, 29, 30). We, therefore, used a megakaryoblast cell line, MEG-01, to assess the role of CRT deficiency and the CRT_{Del52} mutant on basal cytosolic calcium levels and SERCA inhibition-induced calcium influx into the cytosol. As with the HEK cells (Figure 4), we created a stable CRT knockout clone of MEG-01 cells by CRISPR/Cas9 editing for cytosolic calcium measurements. The cells were subsequently reconstituted with wild-type CRT or CRT_{Del52}. Representative immunoblots are shown to demonstrate the successful knockout and reconstitution (Figure 5A). The wild-type CRT was expressed in the reconstituted MEG-01 CRT-KO cells at levels similar to those in the parental cells (Figure 5A, lanes 3-5 compared with lanes 6-8). Cytosolic free calcium was measured in cells loaded with Fura-2/AM dye in the presence of 2 mM extracellular Ca^{2+}. The ratio of the emission at 510 nm following excitation at 340 and 380 nm was calculated and plotted at baseline and following ER calcium depletion with CPA (Figure 5B). We observed no significant differences in the basal cytosolic calcium levels or CPA-induced calcium release from ER in CRT-KO cells compared to the parental MEG-01 cells (Figure 5C and 5D). Additionally, no significant differences in basal cytosolic calcium were observed in CRT-KO cells compared to those reconstituted with wild-type CRT or CRT_{Del52} (Figure 5E). Furthermore, cytosolic calcium levels in CRT-KO and the two reconstituted cell lines were not statistically different following CPA treatments. However, there is a trend towards an increase in the cytosolic calcium levels in cells reconstituted with wild-type CRT, relative to CRT-KO cells or those expressing CRT_{Del52} (Figure 5F).

SOCE is an important process for restoring ER calcium and maintaining intracellular calcium levels. To understand the effects of CRT deficiency and CRT_{Del52} expression on SOCE induction, Fura-2/AM loaded MEG-01 cells lacking CRT and those reconstituted with wild-type CRT or CRT_{Del52} were used to measure initial baseline cytosolic calcium signals. Subsequently, the changes in cytosolic calcium signals were recorded following ER calcium depletion and SOCE induction (Figure 6A). We observed that CRT-KO cells exhibited a small but significant increase in basal cytosolic calcium levels relative to the parental cells in calcium-free saline (Figure 6A, left panel and 6B). Upon ER calcium depletion, the mean fractional increase in the cytosolic calcium measured in the Ca^{2+}-free saline did not differ significantly in parental cells *vs*. CRT-KO cells. The areas under the curve were also not different for the two cell lines (Figures 6A and 6C). Consistent with the higher basal cytosolic calcium measured in CRT-KO cells in calcium-free saline, SOCE induction was significantly reduced in CRT-KO cells compared to parental cells (Figure 6D). Reconstitution of the CRT-KO cells with either wild-type CRT or CRT_{Del52} tended to reduce basal

cytosolic calcium and induce SOCE (Figure 6A, right panel, 6E and 6G), but both trends were non-significant compared to CRT-KO cells. Importantly, there were no significant differences between the wild-type CRT and CRT_{Del52} reconstituted cells, in either their basal or CPA-induced cytosolic calcium signals or in SOCE (Figures 6E-G).

CRT deficiency induced numerous transcriptional changes to genes within the calcium signaling pathway

As noted in Figures 4 and 6, some of the measured differences between CRT-KO and parental cells are not fully reversed by reconstitution with wild-type CRT, although the trends are maintained. Additionally, $CRT_{Del52\text{-}KDEL}$ had a trend towards lower ER calcium compared to CRT_{Del52} (Figure 4D, right panel). We predicted that there may be other indirect effects of CRT-KO and reconstitution that affect cellular calcium levels and calcium signaling that could explain some of these measured differences. As proof of concept, we undertook bulk RNA-sequencing to determine differential gene expression in MEG-01 parental *vs.* CRT-KO cells. Based on pathway analysis, numerous genes involved in cellular calcium signaling were identified. The volcano plot shows genes that were differentially expressed in CRT-KO MEG-01 compared to parental cells (Figure 7). There were 2515 upregulated and 1286 downregulated genes. Of specific note is the upregulation of inositol 1,4,5-triphosphate receptor type 3 (ITPR3), and ryanodine receptor 1 (RyR1), and the downregulation of ATPase plasma membrane Ca^{2+} transporting 3 (ATP2B3) proteins in CRT-KO MEG-01 cells relative to the parental cells, which function in ER to cytosol or cytosol to extracellular calcium transport (31-33). Additionally, GRp94, which has low affinity calcium binding sites (34, 35) is also upregulated and may serve a compensatory role in buffering calcium in CRT-KO cells. Other key factors, such as the nuclear factor of activated T-cells (NFAT) and calcium/calmodulin-dependent protein kinases (CaMKs) isoforms were identified as being differentially expressed in CRT-KO cells.

Discussion

Calreticulin is a ubiquitously expressed ER luminal calcium-binding chaperone, with a role in ER calcium storage (5, 36). CRT_{Del52} has been reported to have impaired calcium binding using a stains-all dye-based assay (9). However, more quantitative measurements of calcium binding to the low affinity sites of CRT_{Del52} have not been undertaken. In this study, we investigated low affinity calcium binding by wild-type human CRT, CRT_{Del52}, and the truncation mutants $CRT_{(1-351)}$ and $CRT_{(1-339)}$ (Figure 1). Our studies show that wild-type CRT, $CRT_{Del52,}$ and $CRT_{(1-351)}$ exhibit average K_D values of 574.24, 938.82, and 444.34 μM, respectively. No calcium binding is observed for $CRT_{(1-339)}$ (Figure 3 and Table 1). Thus, CRT_{Del52} retains at least some low affinity calcium binding sites. Furthermore, residues 340-349 shared by wild-type CRT and CRT_{Del52} play a major role in the low affinity calcium binding by CRT_{Del52}, as measured by ITC (Figure 3). This finding is consistent with our previous report, which demonstrated low affinity calcium binding to $mCRT_{(1-351)}$ but not to $mCRT_{(1-339)}$ (14), emphasizing the major contributions of the conserved 340-349 residues to the low affinity calcium binding across species.

While the CRT_{Del52} mutant retains at least some low affinity calcium-binding sites, it might still be unable to contribute to ER calcium due to the loss of its KDEL retention sequence (Figure 1). However, there were no significant differences measured in ER calcium levels for CRT-KO cells compared to those reconstituted with wild-type CRT, CRT_{Del52}, or $CRT_{Del52\text{-}KDEL}$, although free basal ER calcium levels were non-significantly elevated in cells reconstituted with wild-type CRT. In contrast, there is a non-significant trend towards even lower ER calcium in cells expressing $CRT_{Del52\text{-}KDEL}$ compared with those expressing CRT_{Del52} (Figure 4D), hinting at the possibility that effects unrelated to actual calcium-binding differences between CRT variants can cause changes to basal ER calcium. These findings of similar ER calcium levels in CRT-KO cells and those reconstituted with wild-type CRT are consistent with prior reports of similar levels of free ER luminal calcium in CRT-KO mouse fibroblasts compared with their wild-type counterparts (3). One study has reported decreased ER calcium levels in a human osteosarcoma cell line expressing CRT_{Del52} compared to those expressing wild-type CRT, following transient transfections (9). The same study suggested the contributions of the P and C-domain of wild type in restoring ER calcium levels in cells expressing CRT_{Del52} (9). While the conditions of those experiments differ from the studies described here which use a CRT-KO background and a different cell line, our findings are consistent with the prediction that any excess free ER calcium generated in cells lacking CRT or sufficient ER calcium binding sites would rapidly diffuse out of the ER and get pumped out of the cell.

Basal and CPA induced cytosolic calcium were also similar between CRT-KO cells and those reconstituted with wild type CRT or CRT_{Del52} at physiological levels of extracellular calcium (Figures 5E-F). Additionally, SOCE activation was similar in CRT-KO cells compared to those reconstituted with wild type CRT or CRT_{Del52} (Figure 6G). Consistent with these findings, in a previous study, no differences were observed in cytosolic calcium levels and SOCE induction in myeloid progenitor 32D cells expressing wild-type CRT and CRT_{Del52} both under conditions of cytokine deprivation and thrombopoietin (TPO)-stimulation (37). While cultured megakaryocytes from MPN patients with *CALR* mutations have SOCE abnormalities compared to healthy control cells (12, 13), sample to sample heterogeneities in primary cells make it difficult to attribute measured differences solely to calcium binding by CRT or its mutants.

The RNA sequencing results (Figure 7) emphasize that, when comparing wild type and CRT-KO cell lines for subcellular calcium levels or responses to SERCA inhibitors (for example, Figures 4 and 6), the measured effects might not be based solely on the abilities of CRT to maintain ER and cytosolic Ca^{2+} levels via its calcium binding, storage and buffering capacity. Rather, many other

accompanying cellular changes could affect subcellular calcium levels and signaling. Not all of the changes might fully reset to the parental levels following reconstitutions, accounting for some of the differences between the effects of parental vs. wild type CRT reconstituted cells. While ITPR3 maintains intracellular calcium homeostasis by releasing calcium out of the ER into the cytosol, overexpression of ITPR3 can induce ER depletion and SOCE (32). In neuroblastoma cells, the loss of IP3R reduces SOCE and is restored upon reconstitution (38, 39). In mouse skeletal muscle myoblasts, cytosolic calcium levels were decreased when RyR1 was inhibited or knocked down (40). The Ca^{2+}-ATPase system, which rapidly pushes calcium out of the cytoplasm across the plasma membrane, is one of the principal mechanisms for keeping intracellular calcium in the sub-micromolar range (41). Downregulation of ATP2B3 in CRT-KO, compared to parental cells (in Figure 7), may regulate the loss of excess cytosolic calcium out of the cells and account for changes in cytosolic calcium levels under some conditions (Figure 6B). Glucose-regulated protein 94, also known as gp96 or HSP90B1, is an ER resident calcium binding protein that serves as a calcium store, and expression of which is responsive to the perturbations of intracellular calcium (34, 42, 43). Increased expression of GRP94 could compensate for the loss of calcium stores in CRT-KO cells. The RNA sequencing data also showed a differential expression of downstream effectors of calcium signaling, NFAT and CAMKs. An increase in cytosolic calcium activates the calmodulin-calcineurin pathway (44). This leads to the formation of calcium-calmodulin complex that activates calcium pumps to push calcium out of the cell, while also activating CAMK to further activate other downstream proteins (45). The RNA Seq data indicated increased expression of NFAT2/4 isoforms as well as CAMK2D in CRT-KO cells (Figure 7). Overall, we can conclude that a number of factors that contribute to the regulation and maintenance of intracellular calcium levels are altered in CRT-KO cells. In this study, the effects of the Del52 mutation upon expression of such factors was not tested, further analyses of which would be best undertaken using relevant primary cells and knock-in cell lines.

In summary, our findings indicate the maintenance of at least some low affinity calcium binding sites in the CRT_{Del52} mutant, and a small, non-significant reduction in ER calcium levels in cells expressing CRT_{Del52} compared wild wild-type CRT expressing cells. Calcium homeostasis and signaling changes induced by CRT deficiency or mutation could involve other calcium signaling mediators.

Acknowledgements

We thank Grace Pagnucco for her contribution to creating the CRISPR/Cas9-engineered HEK293T CRT-KO cells and Arunkumar Venkatesan for the MEG-01 CRT-KO cells. We would like to extend special thanks and appreciation to Chante Liu and Mathewos Biniam Tebeje from the Satin's lab for their support with microscopic calcium measurements.

We thank the Advanced Genomic Core (ACG) at the University of Michigan for conducting the library preparation and next-generation sequencing, as well as the Bioinformatics Core of the University of Michigan Medical School for conducting the RNA sequencing data analysis. We thank Dr. Arthur Sherman for many insightful comments. This work was funded by the National Institute of Health grants (R01 AI123957 to MR and R01DK46409 to LSS) and by the University of Michigan Fast Forward Protein Folding Diseases Initiative.

REFERENCES

1. Kozlov G, Pocanschi CL, Rosenauer A, Bastos-Aristizabal S, Gorelik A, Williams DB, Gehring K. 2010. Structural basis of carbohydrate recognition by calreticulin. *J Biol Chem* 285: 38612-20
2. Frickel EM, Riek R, Jelesarov I, Helenius A, Wuthrich K, Ellgaard L. 2002. TROSY-NMR reveals interaction between ERp57 and the tip of the calreticulin P-domain. *Proc Natl Acad Sci U S A* 99: 1954-9
3. Nakamura K, Zuppini A, Arnaudeau S, Lynch J, Ahsan I, Krause R, Papp S, De Smedt H, Parys JB, Muller-Esterl W, Lew DP, Krause KH, Demaurex N, Opas M, Michalak M. 2001. Functional specialization of calreticulin domains. *J Cell Biol* 154: 961-72
4. Baksh S, Michalak M. 1991. Expression of Calreticulin in Escherichia-Coli and Identification of Its Ca2+ Binding Domains. *Journal of Biological Chemistry* 266: 21458-65
5. Michalak M. 2024. Calreticulin: Endoplasmic reticulum Ca(2+) gatekeeper. *J Cell Mol Med* 28: e17839
6. Bagur R, Hajnoczky G. 2017. Intracellular Ca(2+) Sensing: Its Role in Calcium Homeostasis and Signaling. *Mol Cell* 66: 780-8
7. Klampfl T, Gisslinger H, Harutyunyan AS, Nivarthi H, Rumi E, Milosevic JD, Them NC, Berg T, Gisslinger B, Pietra D, Chen D, Vladimer GI, Bagienski K, Milanesi C, Casetti IC, Sant'Antonio E, Ferretti V, Elena C, Schischlik F, Cleary C, Six M, Schalling M, Schonegger A, Bock C, Malcovati L, Pascutto C, Superti-Furga G, Cazzola M, Kralovics R. 2013. Somatic mutations of calreticulin in myeloproliferative neoplasms. *N Engl J Med* 369: 2379-90
8. Nangalia J, Massie CE, Baxter EJ, Nice FL, Gundem G, Wedge DC, Avezov E, Li J, Kollmann K, Kent DG, Aziz A, Godfrey AL, Hinton J, Martincorena I, Van Loo P, Jones AV, Guglielmelli P, Tarpey P, Harding HP, Fitzpatrick JD, Goudie CT, Ortmann CA, Loughran SJ, Raine K, Jones DR, Butler AP, Teague JW, O'Meara S, McLaren S, Bianchi M, Silber Y, Dimitropoulou D, Bloxham D, Mudie L, Maddison M, Robinson B, Keohane C, Maclean C, Hill K, Orchard K, Tauro S, Du MQ, Greaves M, Bowen D, Huntly BJP, Harrison CN, Cross NCP, Ron D, Vannucchi AM, Papaemmanuil E, Campbell PJ, Green AR. 2013. Somatic CALR mutations in myeloproliferative neoplasms with nonmutated JAK2. *N Engl J Med* 369: 2391-405
9. Ibarra J, Elbanna YA, Kurylowicz K, Ciboddo M, Greenbaum HS, Arellano NS, Rodriguez D, Evers M, Bock-Hughes A, Liu C, Smith Q, Lutze J, Baumeister J, Kalmer M, Olschok K, Nicholson B, Silva D, Maxwell L, Dowgielewicz J, Rumi E, Pietra D, Casetti IC, Catricala S, Koschmieder S, Gurbuxani S, Schneider RK, Oakes SA, Elf SE. 2022. Type I but Not Type II Calreticulin Mutations Activate the IRE1alpha/XBP1 Pathway of the Unfolded Protein Response to Drive Myeloproliferative Neoplasms. *Blood Cancer Discov* 3: 298-315
10. Putney JW. 2011. Origins of the concept of store-operated calcium entry. *Front Biosci (Schol Ed)* 3: 980-4
11. Cheng KT, Ong HL, Liu X, Ambudkar IS. 2013. Contribution and regulation of TRPC channels in store-operated Ca2+ entry. *Curr Top Membr* 71: 149-79
12. Pietra D, Rumi E, Ferretti VV, Di Buduo CA, Milanesi C, Cavalloni C, Sant'Antonio E, Abbonante V, Moccia F, Casetti IC, Bellini M, Renna MC, Roncoroni E, Fugazza E, Astori C, Boveri E, Rosti V, Barosi G, Balduini A, Cazzola M. 2016. Differential clinical effects of different mutation subtypes in CALR-mutant myeloproliferative neoplasms. *Leukemia* 30: 431-8
13. Di Buduo CA, Abbonante V, Marty C, Moccia F, Rumi E, Pietra D, Soprano PM, Lim D, Cattaneo D, Iurlo A, Gianelli U, Barosi G, Rosti V, Plo I, Cazzola M, Balduini A. 2020.

Defective interaction of mutant calreticulin and SOCE in megakaryocytes from patients with myeloproliferative neoplasms. *Blood* 135: 133-44
14. Wijeyesakere SJ, Gafni AA, Raghavan M. 2011. Calreticulin is a thermostable protein with distinct structural responses to different divalent cation environments. *J Biol Chem* 286: 8771-85
15. Wijeyesakere SJ, Bedi SK, Huynh D, Raghavan M. 2016. The C-Terminal Acidic Region of Calreticulin Mediates Phosphatidylserine Binding and Apoptotic Cell Phagocytosis. *J Immunol* 196: 3896-909
16. Huth JR, Bewley CA, Jackson BM, Hinnebusch AG, Clore GM, Gronenborn AM. 1997. Design of an expression system for detecting folded protein domains and mapping macromolecular interactions by NMR. *Protein Sci* 6: 2359-64
17. Del Cid N, Jeffery E, Rizvi SM, Stamper E, Peters LR, Brown WC, Provoda C, Raghavan M. 2010. Modes of calreticulin recruitment to the major histocompatibility complex class I assembly pathway. *J Biol Chem* 285: 4520-35
18. Mohan HM, Yang B, Dean NA, Raghavan M. 2020. Calreticulin enhances the secretory trafficking of a misfolded alpha-1-antitrypsin. *J Biol Chem* 295: 16754-72
19. Venkatesan A, Geng J, Kandarpa M, Wijeyesakere SJ, Bhide A, Talpaz M, Pogozheva ID, Raghavan M. 2021. Mechanism of mutant calreticulin-mediated activation of the thrombopoietin receptor in cancers. *J Cell Biol* 220
20. Bashirova AA, Viard M, Naranbhai V, Grifoni A, Garcia-Beltran W, Akdag M, Yuki Y, Gao X, O'HUigin C, Raghavan M, Wolinsky S, Bream JH, Duggal P, Martinson J, Michael NL, Kirk GD, Buchbinder SP, Haas D, Goedert JJ, Deeks SG, Fellay J, Walker B, Goulder P, Cresswell P, Elliott T, Sette A, Carlson J, Carrington M. 2020. HLA tapasin independence: broader peptide repertoire and HIV control. *Proc Natl Acad Sci U S A* 117: 28232-8
21. Suzuki J, Kanemaru K, Ishii K, Ohkura M, Okubo Y, Iino M. 2014. Imaging intraorganellar Ca2+ at subcellular resolution using CEPIA. *Nat Commun* 5: 4153
22. Araki M, Yang Y, Masubuchi N, Hironaka Y, Takei H, Morishita S, Mizukami Y, Kan S, Shirane S, Edahiro Y, Sunami Y, Ohsaka A, Komatsu N. 2016. Activation of the thrombopoietin receptor by mutant calreticulin in CALR-mutant myeloproliferative neoplasms. *Blood* 127: 1307-16
23. Arshad N, Cresswell P. 2018. Tumor-associated calreticulin variants functionally compromise the peptide loading complex and impair its recruitment of MHC-I. *J Biol Chem* 293: 9555-69
24. Chachoua I, Pecquet C, El-Khoury M, Nivarthi H, Albu RI, Marty C, Gryshkova V, Defour JP, Vertenoeil G, Ngo A, Koay A, Raslova H, Courtoy PJ, Choong ML, Plo I, Vainchenker W, Kralovics R, Constantinescu SN. 2016. Thrombopoietin receptor activation by myeloproliferative neoplasm associated calreticulin mutants. *Blood* 127: 1325-35
25. Masubuchi N, Araki M, Yang Y, Hayashi E, Imai M, Edahiro Y, Hironaka Y, Mizukami Y, Kihara Y, Takei H, Nudejima M, Koike M, Ohsaka A, Komatsu N. 2020. Mutant calreticulin interacts with MPL in the secretion pathway for activation on the cell surface. *Leukemia* 34: 499-509
26. Liu P, Zhao L, Loos F, Marty C, Xie W, Martins I, Lachkar S, Qu B, Waeckel-Enee E, Plo I, Vainchenker W, Perez F, Rodriguez D, Lopez-Otin C, van Endert P, Zitvogel L, Kepp O, Kroemer G. 2020. Immunosuppression by Mutated Calreticulin Released from Malignant Cells. *Mol Cell* 77: 748-60 e9
27. Pecquet C, Papadopoulos N, Balligand T, Chachoua I, Tisserand A, Vertenoeil G, Nedelec A, Vertommen D, Roy A, Marty C, Nivarthi H, Defour JP, El-Khoury M, Hug E, Majoros A, Xu E, Zagrijtschuk O, Fertig TE, Marta DS, Gisslinger H, Gisslinger B, Schalling M, Casetti I, Rumi E, Pietra D, Cavalloni C, Arcaini L, Cazzola M, Komatsu N, Kihara Y, Sunami Y, Edahiro Y,

Araki M, Lesyk R, Buxhofer-Ausch V, Heibl S, Pasquier F, Havelange V, Plo I, Vainchenker W, Kralovics R, Constantinescu SN. 2023. Secreted mutant calreticulins as rogue cytokines in myeloproliferative neoplasms. *Blood* 141: 917-29

28. Zhang IX, Raghavan M, Satin LS. 2020. The Endoplasmic Reticulum and Calcium Homeostasis in Pancreatic Beta Cells. *Endocrinology* 161
29. Marty C, Pecquet C, Nivarthi H, El-Khoury M, Chachoua I, Tulliez M, Villeval JL, Raslova H, Kralovics R, Constantinescu SN, Plo I, Vainchenker W. 2016. Calreticulin mutants in mice induce an MPL-dependent thrombocytosis with frequent progression to myelofibrosis. *Blood* 127: 1317-24
30. Li J, Prins D, Park HJ, Grinfeld J, Gonzalez-Arias C, Loughran S, Dovey OM, Klampfl T, Bennett C, Hamilton TL, Pask DC, Sneade R, Williams M, Aungier J, Ghevaert C, Vassiliou GS, Kent DG, Green AR. 2018. Mutant calreticulin knockin mice develop thrombocytosis and myelofibrosis without a stem cell self-renewal advantage. *Blood* 131: 649-61
31. Stafford N, Wilson C, Oceandy D, Neyses L, Cartwright EJ. 2017. The Plasma Membrane Calcium ATPases and Their Role as Major New Players in Human Disease. *Physiol Rev* 97: 1089-125
32. Yue L, Wang L, Du Y, Zhang W, Hamada K, Matsumoto Y, Jin X, Zhou Y, Mikoshiba K, Gill DL, Han S, Wang Y. 2020. Type 3 Inositol 1,4,5-Trisphosphate Receptor is a Crucial Regulator of Calcium Dynamics Mediated by Endoplasmic Reticulum in HEK Cells. *Cells* 9
33. Wang X, Chen X, Tang Z, Yao W, Liu X, Wei R, Wang X, Ka W, Sun D, He D, Wen Z, Chien S. 2009. Ryanodine receptor 1 mediates Ca2+ transport and influences the biomechanical properties in RBCs. *J Biomech* 42: 2774-9
34. Nigam SK, Goldberg AL, Ho S, Rohde MF, Bush KT, Sherman M. 1994. A set of endoplasmic reticulum proteins possessing properties of molecular chaperones includes Ca(2+)-binding proteins and members of the thioredoxin superfamily. *J Biol Chem* 269: 1744-9
35. Cala SE, Jones LR. 1994. GRP94 resides within cardiac sarcoplasmic reticulum vesicles and is phosphorylated by casein kinase II. *J Biol Chem* 269: 5926-31
36. Venkatesan A, Satin LS, Raghavan M. 2021. Roles of Calreticulin in Protein Folding, Immunity, Calcium Signaling and Cell Transformation. *Prog Mol Subcell Biol* 59: 145-62
37. Bhuria V, Franz T, Baldauf C, Bottcher M, Chatain N, Koschmieder S, Brummendorf TH, Mougiakakos D, Schraven B, Kahlfuss S, Fischer T. 2024. Activating mutations in JAK2 and CALR differentially affect intracellular calcium flux in store operated calcium entry. *Cell Commun Signal* 22: 186
38. Sampieri A, Santoyo K, Asanov A, Vaca L. 2018. Association of the IP3R to STIM1 provides a reduced intraluminal calcium microenvironment, resulting in enhanced store-operated calcium entry. *Sci Rep* 8: 13252
39. Chakraborty P, Deb BK, Arige V, Musthafa T, Malik S, Yule DI, Taylor CW, Hasan G. 2023. Regulation of store-operated Ca(2+) entry by IP(3) receptors independent of their ability to release Ca(2). *Elife* 12
40. Qiu K, Wang Y, Xu D, He L, Zhang X, Yan E, Wang L, Yin J. 2022. Ryanodine receptor RyR1-mediated elevation of Ca(2+) concentration is required for the late stage of myogenic differentiation and fusion. *J Anim Sci Biotechnol* 13: 9
41. Strehler EE, Caride AJ, Filoteo AG, Xiong Y, Penniston JT, Enyedi A. 2007. Plasma membrane Ca2+ ATPases as dynamic regulators of cellular calcium handling. *Ann N Y Acad Sci* 1099: 226-36
42. Biswas C, Ostrovsky O, Makarewich CA, Wanderling S, Gidalevitz T, Argon Y. 2007. The peptide-binding activity of GRP94 is regulated by calcium. *Biochem J* 405: 233-41

43. Drummond IA, Lee AS, Resendez E, Jr., Steinhardt RA. 1987. Depletion of intracellular calcium stores by calcium ionophore A23187 induces the genes for glucose-regulated proteins in hamster fibroblasts. *J Biol Chem* 262: 12801-5
44. Park YJ, Yoo SA, Kim M, Kim WU. 2020. The Role of Calcium-Calcineurin-NFAT Signaling Pathway in Health and Autoimmune Diseases. *Front Immunol* 11: 195
45. Gwack Y, Feske S, Srikanth S, Hogan PG, Rao A. 2007. Signalling to transcription: store-operated Ca2+ entry and NFAT activation in lymphocytes. *Cell Calcium* 42: 145-56

Figures and legends

A

```
mCRT      DGEWEPPVIQNPEYKGEWKPRQIDNPDYKGTWIHPEIDNPEYSPDANIYAYDSFAVLGLD 300
hCRT      DGEWEPPVIQNPEYKGEWKPRQIDNPDYKGTWIHPEIDNPEYSPDPSIYAYDNFGVLGLD 300
Ins5      DGEWEPPVIQNPEYKGEWKPRQIDNPDYKGTWIHPEIDNPEYSPDPSIYAYDNFGVLGLD 300
Del52     DGEWEPPVIQNPEYKGEWKPRQIDNPDYKGTWIHPEIDNPEYSPDPSIYAYDNFGVLGLD 300
          ******************************************** .*****.*.*****

                                                 340      349
mCRT      LWQVKSGTIFDNFLITNDEAYAEEFGNETWGVTKAAEKQMKDKQDEEQRLKEEEEDKKRK 360
hCRT      LWQVKSGTIFDNFLITNDEAYAEEFGNETWGVTKAAEKQMKDKQDEEQRLKEEEEDKKRK 360
Ins5      LWQVKSGTIFDNFLITNDEAYAEEFGNETWGVTKAAEKQMKDKQDEEQRLKEEEEDKKRK 360
Del52     LWQVKSGTIFDNFLITNDEAYAEEFGNETWGVTKAAEKQMKDKQDEEQR---------- 349
         ************************************************

mCRT      EEEEAEDKEDDDDRDEDEDEEDEK---EEDEEESPGQAKDEL-----------  399
hCRT      EEEEAEDKEDDEDKDEDEEDEEDK--EEDEEEDVPGQAKDEL-----------  400
Ins5      EEEEAEDNCRRMMRTKMRMRRMRRTRRKMRRKMSPARPRTSCREACLQGWTEA  413
Del52     --------TRRMMRTKMRMRRMRRTRRKMRRKMSPARPRTSCREACLQGWTEA  394
                     : : .  .  :   :  .:  *.: : .
```

Figure 1: Sequence alignments of the C-terminal residues of murine and human calreticulin (mCRT and hCRT), MPN-linked CRT mutants Ins5 and Del52. Multiple sequence alignment using Clustal Omega was employed to compare C-domain sequences of mature mCRT, hCRT, Del52, and Ins5 proteins. Acidic residues (340 – 349) previously implicated in low affinity calcium binding by mCRT that are shared between wild type and both CRT_{Del52} and CRT_{Ins5} are highlighted in green. Additional acidic residues shared just between wild-type CRT and CRT_{Ins5} are shown in red. There are additional acidic residues unique to wild-type CRT. Mature protein numbering is used for the CRT sequences.

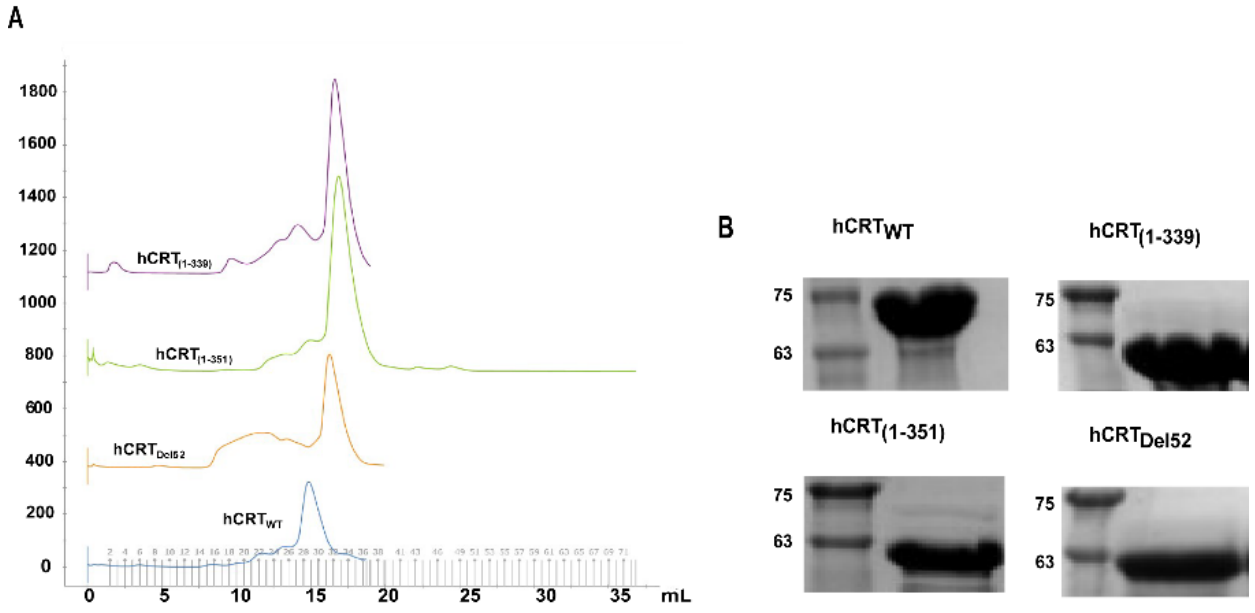

Figure 2: **Purification of recombinant human wild-type CRT, CRT_{Del52}, and C-domain truncation mutants. A)** Representative chromatograms of recombinant human CRT_{WT} ($hCRT_{WT}$), CRT_{Del52}, and the C-domain truncation mutants hCRT $_{(1-351)}$ and hCRT $_{(1-339)}$ purified by gel exclusion chromatography after expression in *E. coli* and initial purification using a nickel resin. **B)** Representative Coomassie blue-stained SDS-PAGE gels of purified proteins that were used for calcium-binding measurements.

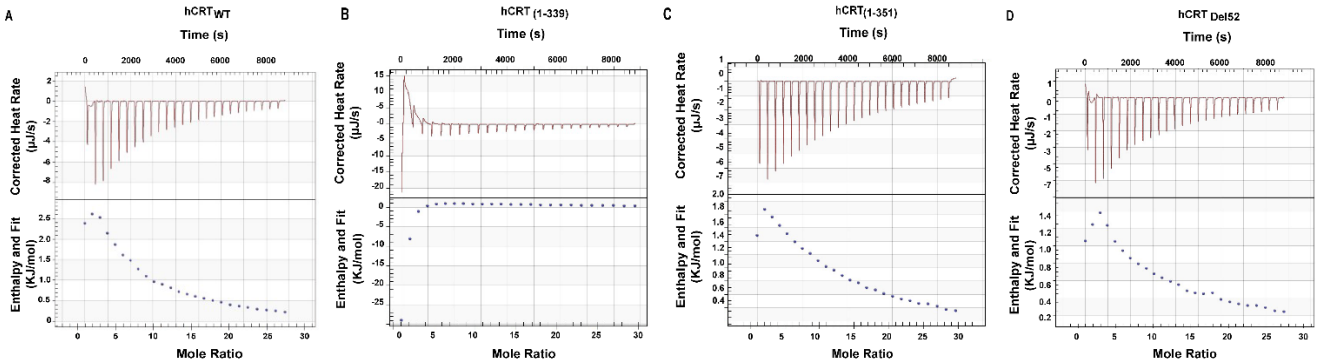

Figure 3: Calcium binding to the low affinity sites of purified human CRT proteins. Low affinity calcium binding by purified $hCRT_{WT}$, CRT_{Del52}, and the indicated truncation mutants was measured using isothermal titration calorimetry. **A-D)** Representative isotherm and fitting curves of calcium binding to the low affinity sites of the wild type and mutant CRT proteins as indicated, measured using isothermal titration calorimetry (ITC). Prior to titration, the proteins were incubated with 50 µM $CaCl_2$ to block the high affinity calcium binding sites. At 37°C, 10 mM $CaCl_2$ was titrated against 100 µM protein. The heat change was measured for 25 injections, and the data were curve-fitted to calculate the dissociation constant, enthalpy, and binding stoichiometry using NanoAnalyzer software. Data replicates and statistical analyses are specified in Table 1.

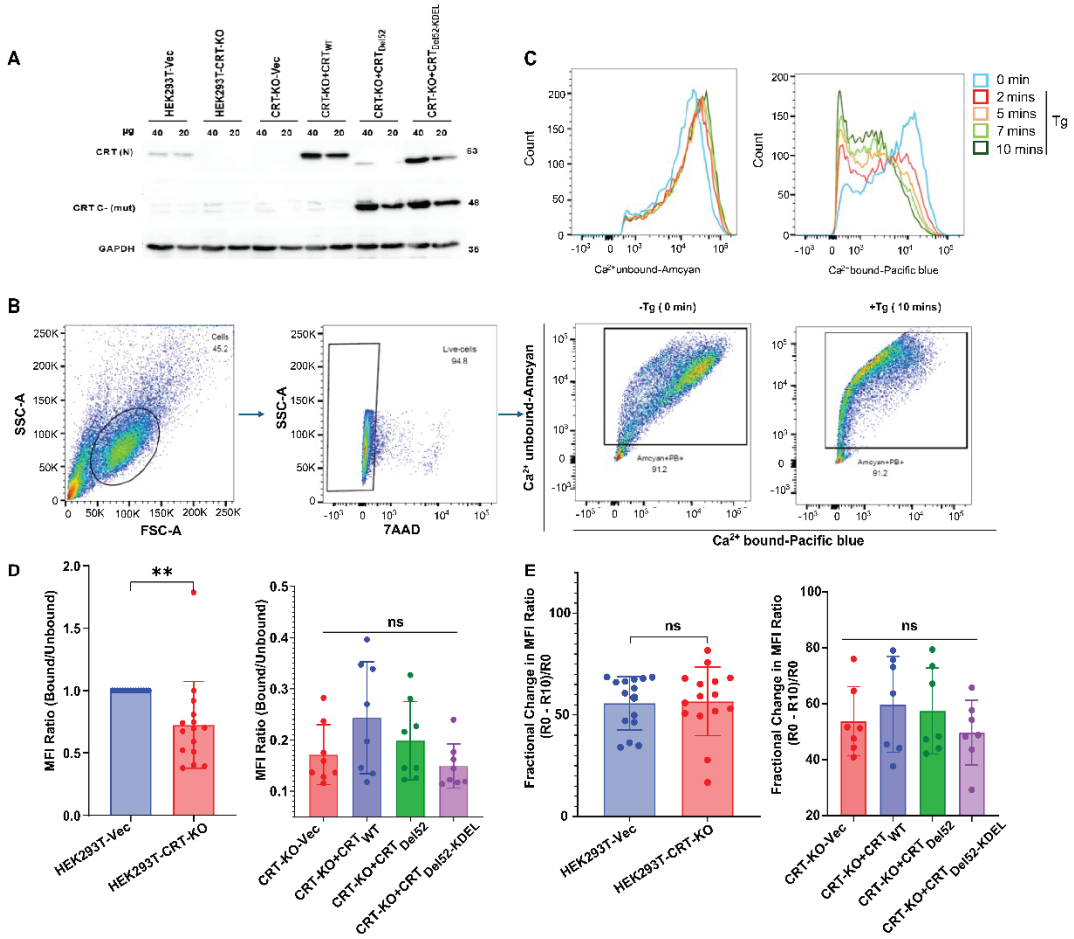

Figure 4: ER calcium measurements in CRT-KO HEK293T cells and those reconstituted with wild-type CRT, CRT_{Del52}, or $CRT_{Del52\text{-}KDEL}$. A) CRISPR-Cas9 editing of HEK cells using lentiviral constructs of calreticulin-targeting gRNA (CRT-KO) or empty vector (HEK-Vec). CRT-KO HEK cells were subsequently reconstituted with wild-type human CRT, CRT_{Del52}, or CRT_{Del52} with a C-terminal KDEL sequence as indicated. Representative blots showing expression levels of CRT in the indicated HEK cells. Cell lysates were subjected to SDS-PAGE followed by immunoblotting. Wild-type CRT, mutant CRT, and GAPDH were detected with anti-CRT (N), anti-CRT C-(mut), and anti-GAPDH antibodies, respectively. **B)** Gating strategy for flow cytometry. HEK-Vec cells transiently transfected with the vector encoding the ratiometric GEM-CEPIA1er probe for 72 hours were used to assess ER calcium levels by flow cytometry based on the measurements of fluorescence emission signals for the Ca^{2+}- bound or unbound probe at 452-455 nm and 498 nm, respectively following excitation with the 405 nm (violet) laser. Transfected cells were gated based on forward (FSC-A) and side scatter (SSC-A), then on 7AAD-negative (live) cells, and further on the cells positive for the calcium-bound or unbound probe signals. Representative dot plots of changes in fluorescence intensities in response to treatment with thapsigargin (Tg), a SERCA inhibitor, before (0 mins) or after (10 mins) treatment, are shown. **C)** Representative histograms showing changes to Ca^{2+}-bound and unbound signals at different time points following Tg treatment of cells. Mean fluorescence intensities (MFI) for Ca^{2+}-bound and unbound signals were used to calculate the bound/unbound ratios at different time points. **D and E)** The basal free ER calcium signals were measured as bound/unbound MFIs ratios from the corresponding histograms of CRT-KO or HEK-Vec cells (D, left panel) or CRT-KO cells reconstituted with the indicated CRT constructs (D, right panel). The fractional changes in ER calcium signals in response to Tg were measured at different time points in the indicated cells (E). The fractional change ratios were normalized to the baseline and calculated by subtracting the ratio at 10 mins from the ratio at 0 mins (R0-R10/R0)x100. Multiple comparisons among groups were analyzed using one-way ANOVA with Tukey's test. Statistical significance was determined by p-value ≤ 0.05 using GraphPad Prism. ns, not significant; ** $p < 0.01$. All measurements were undertaken in the presence of 2 mM extracellular Ca^{2+}. Data shown in D and E are based on 7-15 independent experiments as indicated by the individual data points within the graphs. GAPDH, glyceraldehyde-3-phosphate dehydrogenase; SDS-PAGE, sodium dodecyl sulfate-polyacrylamide gel electrophoresis.

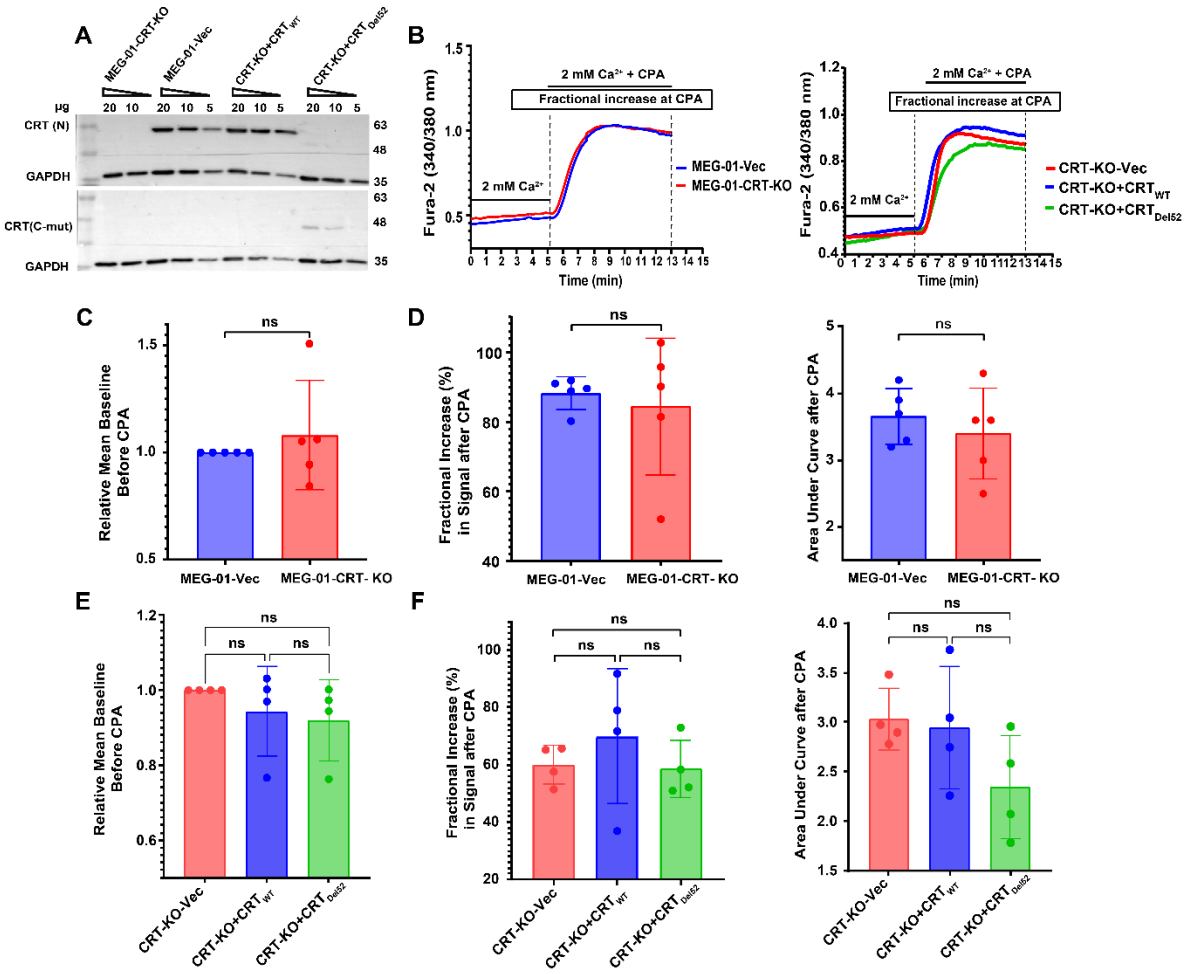

Figure 5: Measurements of cytosolic calcium levels in megakaryoblastic (MEG-01) parental cells, CRT-KO cells, or those reconstituted with wild-type CRT or CRT_{Del52} Cells in 2 mM extracellular Ca^{2+}. were loaded with the Fura-2/AM dye, and the ratio of the signals was calculated following excitation at 340 and 380 nm and emission at 510 nm. **A)** CRISPR-Cas9 editing of MEG-01 cells using lentiviral constructs encoding calreticulin-targeting gRNA (CRT-KO) or empty vector (Vec). CRT-KO MEG-01 cells were subsequently reconstituted with viral constructs encoding wild-type human CRT or CRT_{Del52} or transduced with empty vector (Vec) as indicated in the Figure panels. Representative immunoblots of CRT expression in the indicated cells detected by the anti-CRT(N) and anti-CRT(C-mut) antibodies. **B)** Representative calcium imaging data from indicated cells in the presence of 2 mM extracellular Ca^{2+} and following ER calcium depletion with SERCA inhibitor, cyclopiazonic acid (CPA). **C and E)** Basal cytosolic calcium levels were plotted as the means of ratios of emission signals corresponding to the excitation at 340 and 380 nm. **D and F)** Fractional changes to cytosolic calcium levels in the indicated cell lines, measured following treatment with CPA and total calcium release determined as the area under the curve (AUC), are plotted relative to the baseline following CPA addition. Data shown in C and E are based on 4 or 5 independent measurements, as indicated by the individual data points within the graphs. A paired t-test was used to analyze the mean difference between two groups. Multiple comparisons among groups were analyzed using one-way ANOVA analyses with Tukey's test. Statistical significance was determined by p-value ≤ 0.05 using GraphPad Prism. ns, not significant.

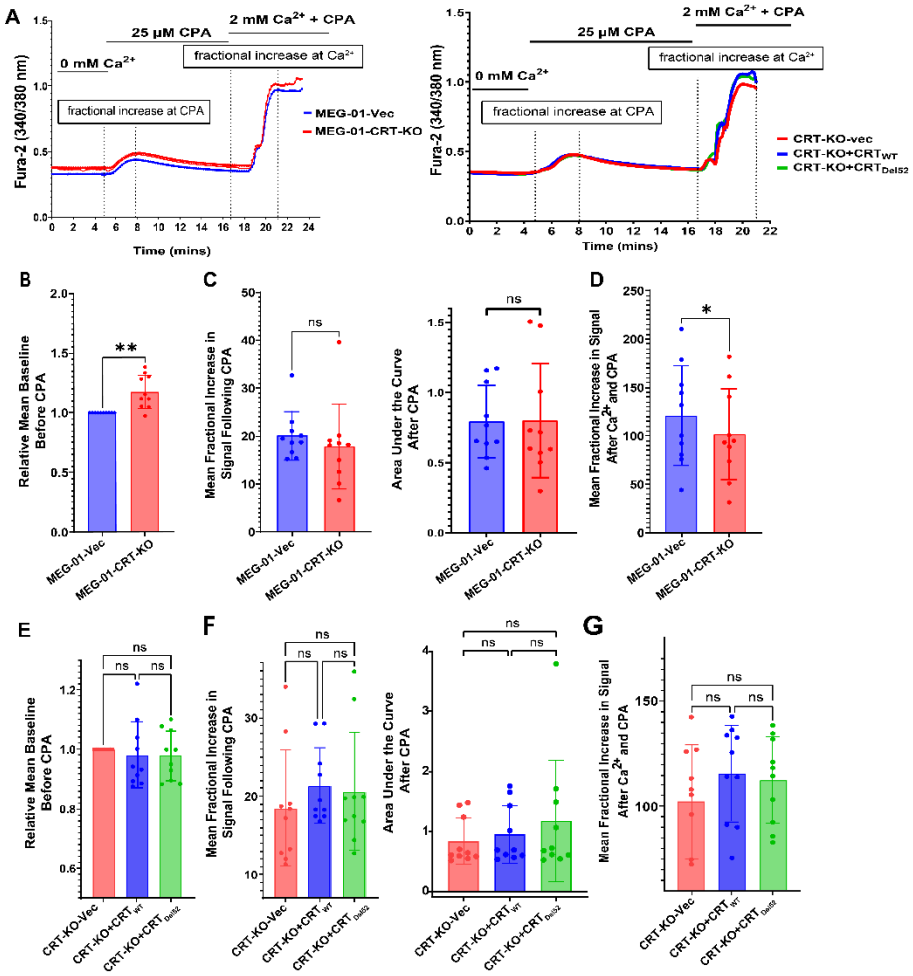

Figure 6: Measurements of cytosolic calcium levels and SOCE in MEG-01 parental cells, CRT-KO, or those reconstituted with wild-type CRT or CRT_{Del52}. Cells were loaded with Fura-2 dye, and the ratio of the 340 nm/380 nm signals was calculated following excitation at 340 and 380 nm and emission at 510 nm. **A)** Representative calcium imaging data from cells in the absence of extracellular calcium, followed by the addition of CPA, and subsequent addition of extracellular calcium with CPA as indicated. **B and E)** Compiled basal cytosolic calcium levels in the indicated cells in the absence of extracellular calcium plotted as the ratios of 340 nm/380 nm signals. **C and F)** Fractional changes to cytosolic calcium and total calcium release measured as the area under the curve (AUC) in the indicated cells following ER calcium depletion with the CPA. **D and G)** Fractional changes to cytosolic calcium following ER calcium depletion with the CPA and subsequent addition of extracellular calcium with CPA. Data are plotted as a fractional increase relative to baseline following CPA addition. SOCE in the indicated cells is plotted as the fractional increase in signal following the addition of 2 mM extracellular calcium in the presence of CPA. Data shown are based on 10 independent measurements. Comparisons were performed by paired t-test and one-way ANOVA analysis using GraphPad Prism. Statistical significance is based on a p-value≤0.05. ns, not significant; * $p < 0.05$, ** $p < 0.01$.

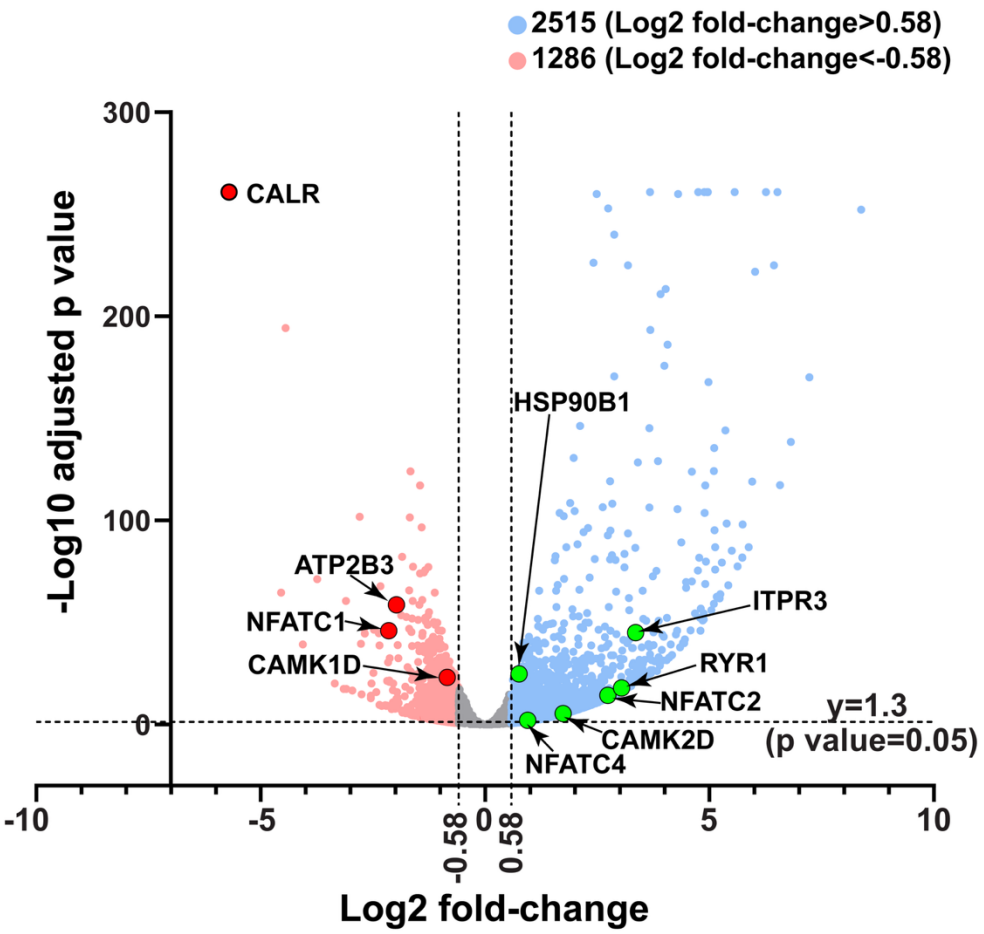

Figure 7: **Volcano plot of changes to expression of genes in the calcium signaling pathway in CRT-KO MEG-01 cells compared to parental MEG-01 cells**. RNA sequencing analyses identified upregulated genes (blue) and downregulated genes (red) in CRT-KO cells compared with parental cells. Genes related to calcium signaling have been highlighted and labeled in the volcano plot.

Table 1: Calorimetric data on measurement of calcium binding to the low affinity binding site of recombinant purified CRT.

Recombinant CRT proteins/Isothermal calorimetric measurement	ΔH (k/mol)	n (mol)	Dissociation constant - K_D (μM)
CRT_{WT}	7.88 ± 2.15	5.40 ± 1.31	574.24 ± 109.93
$CRT_{(1-351)}$	79.82 ± 32.55	2.59 ± 1.56	444.34 ± 139.99
$CRT_{(1-339)}$		No binding	
CRT_{Del52}	3.89 ± 1.36	7.73 ± 1.81	938.82 ± 275.89

Calorimetric data are represented as the mean ± S.E. Data shown are averages from 3 or 5 independent replicates